Anthropogenic warming forces extreme annual glacier mass loss

Lauren J. Vargo[1,2,*], Brian M. Anderson[1], Ruzica Dadić[1], Huw J. Horgan[1,2], Andrew N. Mackintosh[3], Andrew D. King[4], and Andrew M. Lorrey[5]

[1]Antarctic Research Centre, Victoria University of Wellington, Wellington, 6140, New Zealand

[2]School of Geography, Environment and Earth Sciences, Victoria University of Wellington, Wellington, 6140, New Zealand

[3]School of Earth, Atmosphere & Environment, Monash University, Melbourne, 3800, Victoria, Australia

[4]School of Earth Sciences and ARC Centre of Excellence for Climate Extremes, University of Melbourne, Melbourne, 3010, Victoria, Australia

[5]National Institute of Water and Atmospheric Research, Auckland, 1010, New Zealand

[*]lauren.vargo@vuw.ac.nz

Glaciers are unique indicators of climate change. While global-scale glacier decline in recent decades has been attributed to anthropogenic forcing[1], direct links between human influence on climate and years of extreme glacier mass loss have not been documented. Here we address this gap by applying event attribution methods[2] to calculate the anthropogenic influence on extreme glacier mass-loss years at a regional scale, targeting the highest observed mass-loss years (2011 and 2018) across New Zealand's Southern Alps. We simulate glacier mass balance using temperature and precipitation from multi-model[3] and single-model[4] ensembles of climate model output. We show that measured extreme mass-loss was at least 6 times (in 2011) and 10 times (in 2018) (>90% confidence) more likely to occur with anthropogenic forcing than without. This increased likelihood is driven by present-day temperatures ∼1.0°C above the pre-industrial average[3–5], confirming a connection between rising anthropogenic greenhouse gases, warming temperatures, and high annual ice loss. Glaciers will likely continue to melt and retreat under present and future climate conditions[6]. As warming and extreme heat events continue and intensify[7–10], we expect more extreme glacier mass-loss years, with increased fingerprints of human influence in the coming decades.

Glaciers worldwide are exhibiting historically-unprecedented retreat and mass loss[11]. Global glacier retreat, based on length records spanning decades to centuries[11], is often presented as evidence of anthropogenic climate change. Formal

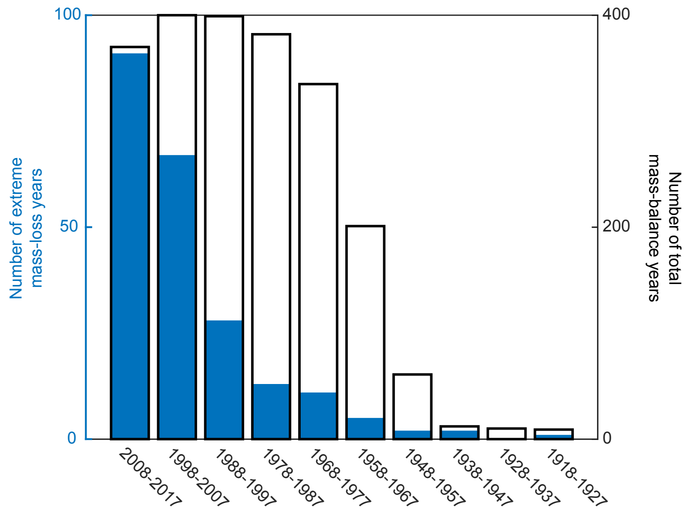

Figure 1. Increasing extreme mass-loss measurements in recent decades. The number of extreme mass-loss years per decade (blue) for the 41 glaciers with mass-balance records of at least 30 years[11], compared with the number of annual measurements from all 41 glaciers per decade (black outline, white fill). Extreme mass-loss years are defined as the 90th percentile of negative measured mass balances from the entire time-series for each glacier.

statistical assessment has shown that centennial-scale retreat of glaciers around the world is categorical evidence of climate change[12]. However, glacier length is a result of mass balance integrated over varying timescales for glaciers with different response times[13]. The use of glacier length changes as climate indicators is further complicated by ice dynamics[14]. Glacier retreat therefore reflects climate trends occurring on different timescales, whereas mass balance directly reflects the response of glaciers to changes in climate[14]. Attribution of global glacier mass loss to anthropogenic forcing has been carried out on decadal timescales, providing evidence of long-term climate change[1]. However, the previously employed attribution methods do not accurately resolve each individual region[1]. The methods also require long-term records of mass-balance measurements[1], but records over 30 years are currently available for only 41 glaciers worldwide, and are almost exclusively in the Northern Hemisphere[11]. Using long-term records for attribution also dampens extreme mass-loss years that have become more prevalent in recent decades (Fig. 1).

Event attribution[2] — using model simulations with and without human-induced forcings to calculate the anthropogenic influences on extreme events — has previously been applied to extreme climate events including heat, drought, and rainfall[8,15]. Application of event attribution methods to annual glacier mass change will facilitate the ongoing assessment of human impacts on global glacier change. This is especially important as glacier retreat will likely accelerate in the future[6,16–18], contributing to sea level rise[6,16–18] and impacting water resources, biodiversity, ecosystems, and human societies[10,19,20]. Here, we establish a method for attribution of extreme glacier mass-loss years to natural or anthropogenic forcings. This is done by simulating glacier mass balance using General Circulation Model (GCM) output for natural and anthropogenically-influenced climate scenarios, and comparing simulation results with direct and proxy mass-balance measurements.

To assess the anthropogenic influence on glacier mass loss, we simulate specific mass balance using data from a multi-model ensemble of 16 Coupled Model Intercomparison Project Phase 5 (CMIP5) models[3] (Fig. S.6) and a single-model ensemble with 34 members from the Community Earth System Model Large Ensemble (CESM)[4]. Using the two model ensembles provides a more robust calculation of attribution[21], as CMIP5 accounts for variations across models, and CESM accounts for model internal variability and initial conditions. Climate influenced only by natural forcings, referred to herein as the natural world, is represented by simulations that include radiative forcing at pre-industrial levels and natural variability. Natural-world climate is defined as April 1901 – March 2005 in HistorialNat CMIP5 scenarios[3], and the CESM 1800-year control run, used from April of year 1 – March of year 1800[4]. Representative concentration pathway (RCP) 8.5 simulations, which include natural variability and anthropogenic forcings, represent the present, anthropogenically-modified climate, referred to herein as the present world. Present-world climate is defined as April 2006 – March 2026 in RCP8.5 for both CMIP5 and CESM[3,4]. As we are calculating anthropogenic influences on extreme mass loss occurring in the present day, the natural-world ensembles represent climate without anthropogenic forcing, not past climate. Therefore, the glacier geometry in our simulations is fixed for present-day geometry. To quantify the role of anthropogenic forcings we compare the probability of extreme measured glacier mass loss occurring in the natural world, with the probability of occurrence in the present world. We assess uncertainties using suites of model parameters, and by including the inherent model uncertainty. Confidence intervals, the 5th and 95th percentiles, are calculated by bootstrapping the simulation output. We use the Intergovernmental Panel on Climate Change (IPCC) likelihood scale to present findings within the 5th and 95th percentiles that are 'very likely', defined as >90% probability[22]. See Methods and Supplemental Information for full methodology.

We apply this method to New Zealand glaciers (Fig. S.1), which provide a rare record of glacier change in the Southern Hemisphere[23], and that have had two years in the past decade with especially high mass loss[23–25]. Mass balance is measured directly for only two New Zealand glaciers, Brewster Glacier (since 2005)[24], and Rolleston Glacier (since 2011)[25] (Fig. S.1). Both mass balance records show that 2011 and 2018 were extreme mass-loss years[11]. Indirect mass-balance measurements from Brewster Glacier, Rolleston Glacier, and eight additional glaciers (beginning 1977 – 1980) show that 2011 and 2018 were the two of the highest mass-loss years on record[23]. These measurements were obtained through oblique aerial photos that are taken at the end of each summer to record the end-of-summer-snowline elevation[26], referred to herein as the snowline. We use the snowline as a proxy for the equilibrium line altitude and therefore mass balance[14].

We find that probability of extreme mass loss occurring increases in a climate with anthropogenic forcing for the two glaciers with direct mass-balance measurements (Figs. 2a,b & 3). High mass loss measured at Brewster Glacier in 2011 has a 0 – 0.8% chance of occurring in any given year in a natural world, but 0.2 – 14% chance of occurring in the present world with an anthropogenically-modified climate (Figs. 2a & 3). Mass loss of Brewster Glacier was even greater in 2018 than in 2011. Mass loss equal to or exceeding 2018 measured mass balance has a 0 – 0.2% chance of occurring in a natural world, and 0 – 5.9% chance of occurring in the present world with anthropogenic forcing (Figs. 2a & 3). The high mass losses measured at Rolleston Glacier have <0.1 – 5.9% (in 2011) and <0.1 – 2.1% (in 2018) chances of occurring in the natural world, while similar or greater mass-loss years for Rolleston Glacier have a 1.4 – 36% (in 2011) and 0.3 – 23% (in 2018) chance of occurring in a climate with anthropogenic forcing (Figs. 2b & 3). Probabilities are presented as the 5th – 95th confidence levels. The broader probability distribution for Rolleston Glacier mass balance (Fig. 2b), compared to Brewster Glacier mass balance (Fig. 2a), is due to the higher standard error in the Rolleston Glacier model calibration, which is incorporated in the probability distributions as the inherent model uncertainty (see Methods for details).

By comparing the probability of measured mass loss occurring in the present world with the probability of measured mass loss occurring in the natural world, we calculate the increase in likelihood of extreme mass loss occurring due to human influence (Fig. 3). Measured mass loss at Brewster Glacier is at least 14 times (in 2011) and at least 23 times (in 2018) (>90% confidence level) more likely to occur in a climate influenced by anthropogenic forcing (Fig. 3). Measured mass loss at Rolleston Glacier in 2011 is at least 6 times (>90% confidence level) more likely to occur with anthropogenic forcing, and in 2018 is at least 10 times (>90% confidence level) more likely to occur with anthropogenic forcing (Fig. 3). For both years of extreme mass loss for Brewster Glacier, there are scenarios within the 5 – 95% confidence levels where measured mass balance does occur in the present world, but does not occur at all in the natural world. There are also scenarios, within the uncertainties, for 2018 where the extreme mass loss does not occur in the present world.

Extreme high snowlines, an indirect indicator of extreme mass loss, are also more likely to occur in the present climate compared with the natural climate for Brewster and Rolleston Glaciers (Fig. 2c,d). For Brewster Glacier, extreme mass loss is 4 – 14 times (in 2011) and 4 – 16 times (in 2018) more likely to occur with anthropogenic forcing (Fig. 3). For Rolleston, extreme mass loss is 4 – 12 times (in 2011) and 4 – 11 times (in 2011) more likely to occur with anthropogenic forcing. However, for both glaciers there is a larger increase in likelihoods of mass loss attributed to anthropogenic forcing when mass-balance measurements, compared with snowline measurements, are used (Fig. 3). For example, considering mass loss at Brewster Glacier in 2018, measured mass loss is an average of 350 times, and at least 23 times (>90% confidence level), more likely to occur with anthropogenic forcing. Conversely, the extreme high snowline in 2018 is only an average of 8 times, and at least 4 times (>90% confidence level), more likely to occur with anthropogenic influence (Fig. 3).

While snowlines can provide an estimate of anthropogenic influence, simulating snowlines with a temperature-index model excludes small-scale processes that influence snowlines. Snowlines are subject to local influences, including avalanches, and other processes not captured in the mass-balance model used here. In our model calibrations, approximately one standard deviation, or $\sim$70%, of mass balance measurements fall within the simulated mass balance parameter suite. However, only $\sim$50% of snowline measurements fall within the simulated snowline parameter suite, showing that snowlines are not simulated as accurately as mass balance. The dampened likelihood calculated with snowline measurements highlights that snowlines are not a perfect proxy for mass balance. Extreme mass-loss years at Brewster Glacier have snowlines within 8 ± 5 m elevation of each other, but differences in measured mass balance of almost 0.5 m w.e. (28%) (Table S.4), reflecting previous work that shows the relationship between snowlines and mass balance is nonlinear[24]. Furthermore, the 2011 snowline at Rolleston Glacier is higher (indicating more mass loss) than the 2018 snowline, while the measured mass balance shows higher mass loss in 2018 by $\sim$0.4 m w.e. (20%) (Table S.4). However, snowlines are an established proxy for mass balance[14,27], and they

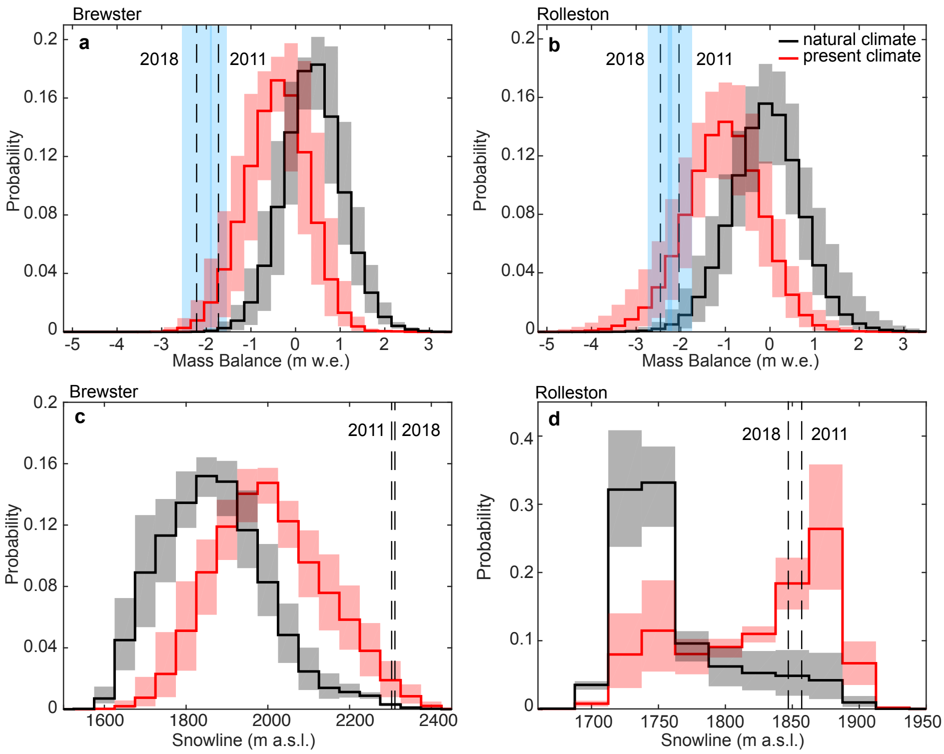

Figure 2. Annual Brewster and Rolleston Glacier mass-balance and snowline probability distributions. Annual mass-balance probability distributions for Brewster Glacier (a) and Rolleston Glacier (b), and annual snowline probability distributions for Brewster Glacier (c) and Rolleston Glacier (d), for natural (black) and present (red) ensembles including CMIP5 and CESM. Bold lines show the mean probabilities calculated using a suite of model parameters, with shading showing the range of probabilities within the suite. Measured 2011 and 2018 mass balances and snowlines are marked with dashed lines. The blue shading shows the uncertainty associated with the mass-balance measurements. For Brewster Glacier these are -1.7 ± 0.2 m w.e. in 2011 and -2.2 ± 0.3 m w.e. in 2018. Uncertainties for Rolleston Glacier are not quantified, so we use an estimated uncertainty of 0.3 m w.e., which is the mean annual uncertainty for Brewster Glacier measurements from 2005 – 2015[24]. Axes on (c) and (d) are different, due to differences in glacier size and elevation range. Note that bin size does not influence the attribution calculations, and that in the snowline calculation, simulated snowlines below the minimum glacier elevation are set to the minimum glacier elevation, and those above the maximum glacier elevation are set to the maximum glacier elevation, these distributions are then expanded after including the inherent model error (see Methods for details).

		Mass balance		Snowline									
		Brewster	Rolleston	Brewster	Rolleston	Salisbury	Park Pass	S. Cameron	Thur-neyson	Vert. 12	Ridge	Glenmary	Vert. 25
Probability of occurring: **Natural**	'11	0.1% (0-0.8%)	0.9% (<0.1-5.9%)	0.2% (0.1-0.4%)	6.3% (2.1-12%)	N/A	3.3% (1.1-7.7%)	10% (4.4-18%)	7.2% (3.3-14%)	1.2% (0.3-3.8%)	2.5% (0.6-6.0%)	13% (7.3-19%)	1.7% (0.4-5.6%)
	'18	<0.1% (0-0.2%)	0.2% (<0.1-2.1%)	0.2% (<0.1-0.4%)	8.2% (2.8-16%)	2.5% (1.1-5.1%)	8.3% (3.5-17%)	7.1% (2.9-13%)	0.8% (0.3-1.5%)	1.5% (0.4-4.7%)	2.6% (0.6-6.2%)	8.5% (4.5-12%)	1.7% (0.4-5.6%)
Probability of occurring: **Present**	'11	3.3% (0.2-14%)	12% (1.4-36%)	1.7% (0.7-3.5%)	39% (25-54%)	N/A	26% (15-41%)	43% (28-57%)	30% (19-39%)	12% (6.1-25%)	14% (4.9-25%)	37% (25-48%)	15% (7.5-28%)
	'18	0.6% (0-5.9%)	5.0% (0.3-23%)	1.5% (0.5-3.0%)	46% (31-63%)	27% (16-42%)	42% (28-59%)	35% (21-48%)	6.4% (2.5-9.2%)	15% (7.7-30%)	15% (5.1-26%)	27% (17-38%)	30% (7.5-28%)
Increase in likelihood	'11	39 (14-only pres)	13 (6-69)	8 (4-14)	6 (4-12)	N/A	8 (5-15)	4 (3-7)	4 (3-6)	11 (7-31)	6 (4-11)	3 (2-4)	9 (6-21)
	'18	350 (23-only pres)	31 (10-190)	8 (4-16)	6 (4-11)	11 (8-16)	5 (3-8)	5 (4-8)	8 (6-12)	10 (6-20)	6 (4-11)	3 (3-4)	9 (6-21)

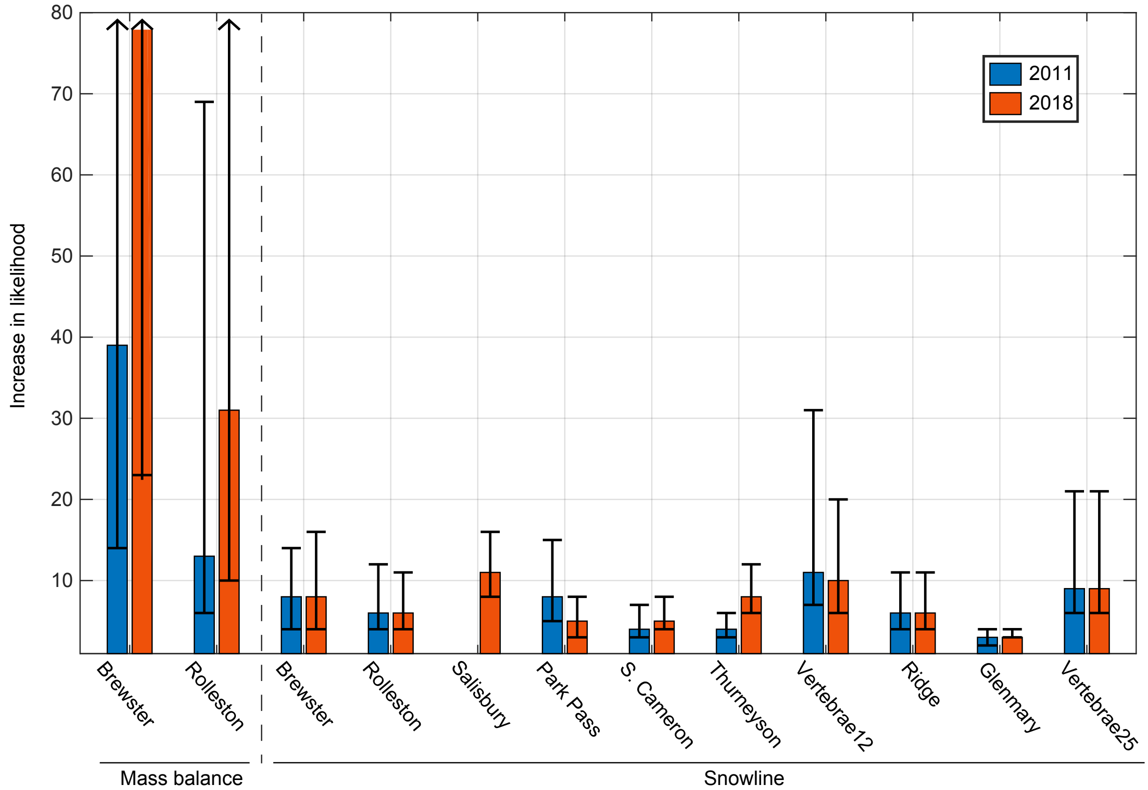

Figure 3. Probabilities and likelihoods of glacier mass loss with natural and anthropogenic forcing. Top: The probability of high mass loss occurring in natural and present worlds, and the increase in likelihood (ratio of present probability to natural probability). Values highlighted in red are discussed in detail in the text. Mean values are presented, with the 5th–95th percentile confidence intervals shown in parentheses. The uncertainty in measured mass balance is also included in mass balance probability and likelihood calculations. The quantifiable uncertainties in snowline elevations is negligible (<1 m). **Bottom:** The increase in likelihood of glacier mass loss occurring with anthropogenic forcing. Error bars show the 5th–95th percentile confidence intervals. Arrows indicate an increase in likelihood of over 80 times. Note the y axis starts at 1, corresponding to no change in likelihood. There is no measurement from Salisbury Glacier in 2011.

provide estimates of inter-annual mass-balance changes for more glaciers than field-based measurements could feasibly include. The agreement between mass balance and snowlines, that high mass loss is more likely with human influence (Fig. 3), shows that snowlines can be useful for estimating anthropogenic influence on extreme glacier mass loss when direct measurements are not available.

We therefore apply the same analysis to eight glaciers where only snowline measurements are available. All eight of the glaciers show an increase in probabilities and likelihoods of extreme mass loss occurring with anthropogenic forcing (Figs. 3, 4). The differences in annual snowline probability distributions (Fig. 4) are largely influenced by differences in glacier size and elevation range. Increases in likelihood of high snowlines occurring with anthropogenic forcing range from an average of 3 times (Glenmary Glacier, 2011) to 11 times (Salisbury Glacier, 2018 and Vertebrae12 Glacier, 2011) (Fig. 3).

Changes in glacier mass balance depend on changes in accumulation and melt, which are largely driven by temperature and precipitation variations[14]. Previous work has shown that New Zealand glacier mass balance is largely influenced by air temperatures, which reflect regional sea surface temperatures and atmospheric circulation patterns, with precipitation being less important in driving mass changes[28]. In our experiment setup, we use temperature and precipitation differences from the GCM ensembles between natural and present worlds, which are adjusted using a regional reanalysis. In the temperature data, averaged for the ten glacier domains, present-world temperatures are 1.0°C (0.4 – 1.7°C across ensemble members) higher than natural-world temperatures (Fig. S.6). This difference in adjusted temperature between natural and present worlds is equal to the change in measured New Zealand temperatures over the last century of $+1.00\pm0.25$°C[5]. The precipitation data shows increasing precipitation in the present world in 45 of the 50 climate models (Fig. S.6). In our mass-balance calculation, precipitation is only included in the accumulation calculation. Increasing precipitation therefore leads to either more positive mass balance if temperatures are below 1°C, or no change in mass balance if temperatures are equal to or above 1°C[29] (see Methods for description). Therefore, it is the temperature increase in the present-world simulations, not precipitation, that drives the increase in likelihood of extreme annual mass loss occurring with anthropogenic forcing.

We have provided a framework for calculating the influence of natural and anthropogenic forcing on annual glacier mass loss or mass gain at a regional scale. This framework can be replicated elsewhere for glaciers with direct mass-balance records. For attribution of mass change over a single year, this framework only requires climate data, and short-term mass-balance data for calibration of the mass-balance model. It can therefore be applied to glaciers worldwide, instead of being limited to glaciers with long-term mass-balance records that are largely situated in the Northern Hemisphere. We show that snowlines can be used to get a broader picture of anthropogenic influence when mass-balance measurements are not available. However, direct mass-balance measurements provide more accurate attributions, as 1) snowlines are not a perfect proxy for mass balance, and 2) simulating snowlines with a temperature-index model does not capture all of the small-scale processes that influence snowlines.

Our results show that extreme annual glacier mass loss is much more likely to occur with anthropogenic forcing. For the two New Zealand glaciers with direct mass-balance measurements, we show that extreme mass-loss was at least 6 times (in 2011) and 10 times (in 2018) (>90% confidence) more likely to occur with anthropogenic influence than without. The increase

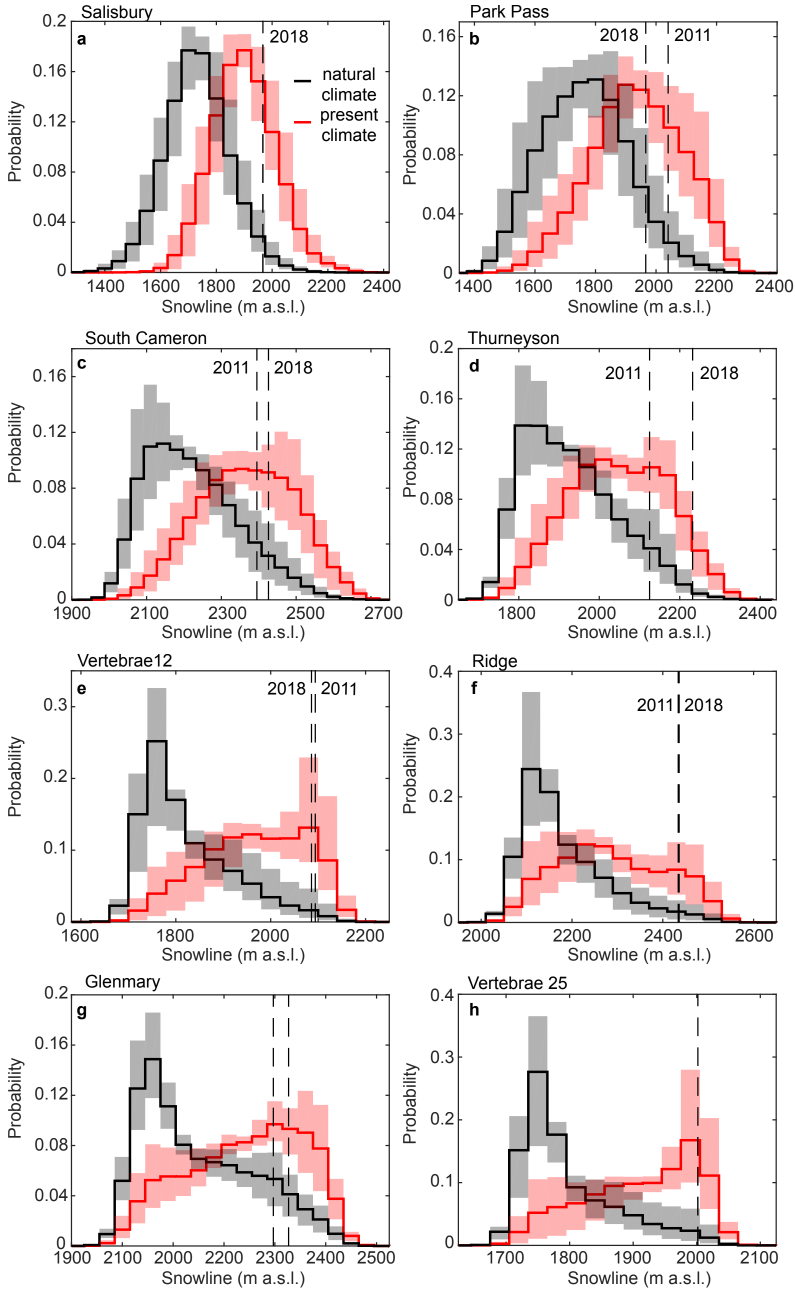

Figure 4. Annual snowline probability distributions. Annual snowline probability distributions for natural (black) and present (red) climate ensembles including CMIP5 and CESM, ordered in decreasing glacier elevation range from a) through h). Bold lines show the mean probabilities calculated using a suite of model parameters, with shading showing the range of probabilities within the suite. Measured 2011 and 2018 snowlines are marked with dashed lines. Note that axes are different, due to differences in glacier size and elevation range.

in likelihood of mass loss occurring with anthropogenic influence is driven by modern temperatures ∼1°C above pre-industrial levels[5], highlighting the connection between warming caused by humans and large annual ice loss. As global temperatures continue to rise to 1.5°C or more above pre-industrial levels over the coming decades[9], both the frequency and magnitude of extreme annual mass loss will likely increase, along with the associated anthropogenic signal.

Methods

Figure S.2 shows an overview of the methods and input data used in this work.

Glaciological input data. Snowline elevations have been documented annually at the end of summer (March – April)[14] for 50 glaciers in the Southern Alps, which started between 1977 and 1980 for different glaciers, using oblique aerial photography[26]. From those 50 glaciers, we analyzed the two glaciers with measured mass-balance data, as well as eight others with only snowline measurements. The eight snowline glaciers were selected as those that provided the best spatial coverage of the Southern Alps, had the most continuous records, and are the largest, as some of the 50 glaciers are now nonexistent[23].

Digital elevation models (DEMs) and orthophoto mosaics, generated using structure from motion photogrammetry[30], are used to define the glacier geometry and snowline elevations. Structure from motion photogrammetry involves using automated feature-matching software to overlap multiple photos — taken for this study using handheld Nikon D800E cameras from a small plane — and generate accurate and precise 3-D models of each glacier. The models are georeferenced using locations of each image, which are captured using a GNSS mounted in the plane, and synchronized with the cameras to capture the image timing at better than 1 x 10^{-3} s resolution[30]. We can also georeference orthomosaics and DEMs from images taken previous years with no image locations[30]. This is done by matching the images that have no locations with images of the same glacier that have locations using structure from motion photogrammetry. Snow and ice in all images is masked, so that only the stable bedrock defines the matches, resulting in georeferenced images that originally had no locations.

The images used to define glacier geometry were collected in March 2018. Orthophoto mosaics are 0.1 – 0.5 m resolution, and DEMs were interpolated to 10 m resolution. DEM vertical errors are 0.3 – 1.7 m, largely depending on the image coverage of each glacier[30]. To define glacier geometry, we used DEMs and orthomosaics generated exclusively from 2018 images to most accurately calculate attributions for the mass loss. DEMs and orthomosaics generated from 2011 images are less accurate because fewer images were taken in 2011, and no image locations were collected. Attribution calculations for mass loss in 2011 are also done on the less-accurate 2011 DEM, and the results are near identical to using the more accurate 2018 DEM (see Glacier geometry section in Supplemental Information). We also used the Landcare Research 25 m Digital Elevation Model, interpolated to 10 m, to calculate shading for radiative forcing over each glacier domain, which requires spatial coverage beyond structure from motion photogrammetry DEMs.

For each glacier, we calculated 2011 and 2018 mean snowline elevations by manually digitizing snowlines (the boundary between snow and ice) on 2011 and 2018 orthophoto mosaics, respectively (Fig. S.3). 2018 orthomosaics were generated using 2018 images and 2018 image locations. 2011 orthomosaics were generated using 2011 images, and then georeferenced through matching with the 2018 images, with snow and ice masked out[30]. We then found the mean elevation of the identified snowline points on the 2018 DEM, as the 2011 DEM is less accurate because fewer images were taken in 2011 and no image locations were collected.

Measured mass balance data from Brewster[24] and Rolleston[25] Glaciers are the basis for calculating extreme mass loss probabilities in 2011 and 2018, and for model calibration. Both mass balance surveys involve point measurements of snow depth (from probing) at the end of the accumulation season (November/December), and point measurements of melt (from stakes drilled into the ice) at the end of the ablation season (March/April). For Brewster Glacier, the mean standard deviation over the published record (2005 – 2015) is 300 mm w.e.[24]. Uncertainties are unquantified for Rolleston Glacier, so we use estimated uncertainties of 300 mm w.e. from Brewster Glacier. Snowline elevation measurements beginning in 1981[23] were used to calibrate the modeling of snowline elevations. These snowline elevations were calculated in previous work[23] by manually transcribing the snowline from oblique photographs onto a base map, digitizing the maps, and using the total ablation area and the glacier's area–altitude curve to calculate the mean ELA.

Positive degree day model. Glacier specific mass balance[31] was simulated using a grid-based positive degree-day model, with an additive radiation term in the calculation for total melt[32]. Melt (M) was calculated following:

$$M = M_T T + M_R(1-a)Q \tag{1}$$

using daily positive temperature (T), a temperature melt factor (M_T; mm d^{-1} °C^{-1}), radiation melt factor (M_R; m^2 mm W^{-1} d^{-1}), albedo (a), and incoming shortwave radiation (Q; W m^{-2}). Accumulation was calculated as the total daily precipitation when mean daily temperature is less than 1°C. The model was run on a daily time step over the 10 m-resolution DEM, with specific mass balance calculated as the mean for all grid cells containing the glacier.

Shortwave radiation (Q) was calculated on an hourly time step, which was then averaged for each day. Q and its two components, direct radiation and diffuse radiation, were calculated[33]. Q is a function of top-of-the-atmosphere insolation[34], zenith and azimuth angles of the sun, surrounding topography[35], and cloudiness. Cloudiness was parameterized[36] by calculating a daily cloud factor as the ratio of measured incoming radiation[37] to clear-sky potential incoming radiation. Albedo (a) was modeled using a fresh snow albedo of 0.85 and ice albedo of 0.35[38], following the equation $a = p_1 - p_2 log_{10} T_a$[39], where T_a is the accumulated daily positive temperature since snowfall, p_1 is the albedo of fresh snow, and p_2 is a parameter coefficient for exponentially decreasing albedo, set here to 0.112[39].

We also calculated the snowline to assess the anthropogenic influence on mass loss for glaciers without measured mass-balance data. Snow water equivalent was calculated daily as snow water equivalent of the previous day, plus any daily accumulation and minus any daily melt. If this equation results in a negative snow water equivalent, it is then set to 0. The snowline was then calculated at the end of the mass-balance year as the mean elevation of all grid cells with snow water equivalent between 15 and 150 mm. This range was defined for simulated snowlines to be comparable with measured snowlines.

Differences in glacier size and elevation range influence the snowline probability distributions (Figs. 2c,d & 4). Because measured snowlines cannot be quantified when they are above or below the glacier, we imposed a similar restriction on simulated snowlines — those that fell below the minimum glacier elevation were set to the minimum glacier elevation, and those that fell above the maximum glacier elevation were set to the maximum glacier elevation. As a result, glaciers with small elevation ranges have higher probabilities that their simulated snowlines will be above or below the glacier. This distribution is especially prominent for Rolleston Glacier (Fig. 2d), where there is >50% likelihood that the snowline in the natural simulations will be at the lowest glacier elevation, and >40% likelihood that the snowline in the present simulations will be at the highest glacier elevation.

Regional climate data. We used daily temperature, precipitation, and shortwave radiation from the New Zealand Virtual Climate Station Network (VCSN) data[37,40,41] with a spatial resolution of 0.05°. For each glacier, we used climate data from the VCSN grid box that includes the center of the glacier. Temperature was scaled with elevation to the structure from motion photogrammetry 10 m DEM with seasonal lapse rates for maximum and minimum daily temperatures[41], which we then used to calculate mean daily temperature.

Model calibration. Model calibration is required for the temperature and radiation melt factors, because the degree-day model does not capture all of the complex glacier dynamics and mass-balance processes. Brewster Glacier is the only glacier in this study with weather station data. Comparison of weather station data collected from below Brewster Glacier (2004 – 2008) with VCSN climate for the same period showed VCSN temperature should be reduced by 1.25°C, and precipitation should be increased by a factor of 1.3 to match the weather station data[41,42]. An adjustment to VCSN temperature and precipitation is required for all glaciers except Brewster Glacier, because the gridded meteorological data is not accurate enough on the high-resolution glacier domains[41]. For the calibrations, we performed grid searches to identify parameter combinations resulting in the lowest annual root mean square errors (RMSE) compared with measured mass balance or snowlines. In addition to using the annual RMSE for model calibration, we also compare the mean of each measured series with the mean of each modeled series, adding a second objective in the calibration[43]. We refer to this error in the calibration setup and results as the 'series mean error'. For all glaciers, we use all parameter combinations where the annual RMSE is less than the minimum annual RMSE +50% of the minimum annual RMSE, and the series mean error is also less than +50% of the minimum annual RMSE. This resulted in 9 – 46 parameter combinations for each glacier. Additional details on the setup of the calibrations (Table S.1) and the calibration results (Table S.2, Fig. S.4, Fig. S.5) are in the Supplemental Information.

GCM climate data. For attribution calculations, we used monthly precipitation and 2 m surface air temperature from two different ensembles of General Circulation Model (GCM) output. First, we used a multi-model ensemble: one ensemble member (r1i1p1) for 16 different GCMs (listed in Fig S.6) that are all part of CMIP5[3]. The 16 CMIP5 GCMs were selected as all CMIP5 GCMs with monthly HistoricalNat, Historical, and RCP8.5 simulations. These GCMs, each developed by different scientific groups, simulate global climate for different experiments, including the RCP8.5, historical, and HistoricalNat simulations used here[3]. Natural climate was defined as HistoricalNat simulations April 1901 – March 2005. Present climate with natural and anthropogenic forcing was defined as RCP8.5 April 2006 – March 2026[8]. RCP8.5 was selected because it is the RCP scenario that global emission rate is closest to as of 2018[44,45]. Additionally, the choice of RCP scenario is less important in the early 21st century when other sources dominate model spread, as the runs are initialised in 2006[46]. Second, we used a single-model ensemble: 34 ensemble members from the CESM Large Ensemble[4]. The CESM Large Ensemble is made of one GCM that is run for 34 ensemble members, each with small differences in initial conditions to capture model internal variability[4]. For CESM, natural climate was defined as the fully-coupled 1,800 year-long control run, using March of the first year through April of the last year to simulate 1,799 mass-balance years. Present climate was defined as April 2006 – March 2026 from each RCP8.5 ensemble member. For both the HistoricalNat simulations and the CESM control run, these natural climates are defined by greenhouse gas concentrations at pre-industrial levels[3,4].

The low spatial resolution of GCM simulations (ranging from 0.90°x1.25° to 2.81°x2.81°) leads to systematic biases between GCM output and VCSN data. Because of these biases, instead of driving the glacier model directly with GCM output, there are methods of removing GCM biases while keeping GCM variability[47–49]. We used the 'delta change method'[47,48] with the higher-resolution VCSN climate to remove GCM biases. We calculated monthly GCM-adjusted temperature (T_{mon}) and precipitation (P_{mon}) following:

$$\begin{aligned} T_{mon}(x,y,t) &= T_{VCSN}(x,y,\bar{t_m}) + (T_{GCM}(x,y,t) - T_{GCMbase}(x,y,\bar{t_m})) \\ P_{mon}(x,y,t) &= P_{VCSN}(x,y,\bar{t_m}) * (P_{GCM}(x,y,t)/P_{GCMbase}(x,y,\bar{t_m})) \end{aligned} \tag{2}$$

where $T_{VCSN}(x,y,\bar{t_m})$ is monthly mean VCSN temperature at (x,y) for the 36-year period 1980 – 2015, $T_{GCM}(x,y,t)$ is monthly GCM temperature at (x,y) for each month t (past or present scenarios), and $T_{GCMbase}(x,y,\bar{t_m})$ is monthly mean GCM base temperature at (x,y), calculated from natural climate simulations 1961 – 1990.

The delta change method gives monthly adjusted temperature and precipitation, however, calculated glacier mass balance can be significantly influenced by the temporal resolution[50,51]. We therefore used VCSN data and GCM-adjusted climate to calculate daily variability for temperature (T_{day}) and precipitation (P_{day}) adjusted from previous work[52], following:

$$\begin{aligned} T_{day}(x,y,t) &= (T_{mon}(x,y,t_m) - T_{VCSN}(x,y,t_m)) + T_{VCSN}(x,y,t_d) \\ P_{day}(x,y,t) &= (P_{mon}(x,y,t_m)/P_{VCSN}(x,y,t_m)) \cdot P_{VCSN}(x,y,t_d) \end{aligned} \tag{3}$$

where $T_{VCSN}(x,y,t_d)$ is daily VCSN temperature, being added to the difference between the monthly mean GCM-adjusted temperature (T_{mon}) and monthly mean VCSN temperature ($P_{VCSN}(x,y,t_m)$). For VCSN climate, both daily and monthly, we used the 36-year period 1980 – 2015. For GCM past climate scenarios that are longer than 36 years, the VCSN period was added to the GCM-adjusted climate in a repeating cycle. Daily adjusted precipitation was calculated in the same way as temperature, except for the precipitation adjustment being multiplicative, where temperature is additive.

To test this method, we compared the sum of degree days over 1980 – 2004 calculated for VCSN with those calculated for the Historical CMIP5 GCM simulations with the imposed daily variability. The 16 GCMs have a smaller sum of degree days than VCSN by an average of 1.1%, with individual GCMs ranging from 0.5 – 1.8% fewer degree days than VCSN over the 24-year period. Because the difference between degree day sums between GCMs and VCSN is low, we do not perform any additional bias adjustment.

Uncertainties. Uncertainties include 1) model parameters, 2) the inherent model uncertainty, and 3) the measured mass balance uncertainties. The quantifiable snowline uncertainty is very low (<1 m). The larger errors associated with the snowline, including manually identifying the snowline and local processes, are unquantified. Uncertainties in model parameters are quantified using a suite of parameters for each glacier in the attribution calculations, with 9 – 46 parameter combinations used for each glacier (Fig. S.4). We included the inherent model error in the attribution calculation. For each modeled mass balance (or snowline elevation) value, we redefined that value as 100 values with a Gaussian distribution with the standard deviation of the model standard error. This was done to distribute the uncertainty of each modeled value. The mean probabilities and likelihoods presented in Fig. 3 are the mean values of all modeled mass balance years, and including the suite of parameters and inherent model error.

We estimated the 5th – 95th percent confidence intervals using bootstrapping methods. For each parameter suite and climate scenario, half of all years were randomly sampled with replacement, and this was done 10,000 times[8]. The mass balance uncertainties were also included when calculating the 5th – 95th percent confidence levels.

Data availability. CMIP5 GCM output is available from public repositories, including https://esgf-node.llnl.gov/search/cmip5/. CESM output is available from the CESM/UCAR repository at http://www.cesm.ucar.edu/projects/community-projects/LENS/data-sets.html. VCSN data is available from https://data.niwa.co.nz//home. See Table S.4 for 2011 and 2018 mass-balance and snowline measurements. Snowlines through 2015 are available from National Institute of Water and Atmospheric Research (NIWA) at https://sirg.org.nz/about/annual-end-of-snummer-snowline-survey/. Global glacier mass-balance data in Fig. 1 is available from the World Glacier Monitoring Service.

Code availability. All code is available from https://github.com/lvargo13/glacier_attribution

References

1. Marzeion, B., Cogley, J. G., Richter, K. & Parkes, D. Attribution of global glacier mass loss to anthropogenic and natural causes. *Science* **345**, 919–921 (2014).

2. King, A. D. Attributing changing rates of temperature record breaking to anthropogenic influences. *Earth's Futur.* **5**, 1156–1168 (2017).

3. Taylor, K. E., Stouffer, R. J. & Meehl, G. A. An overview of CMIP5 and the experiment design. *Bull. Am. Meteorol. Soc.* **93**, 485–498 (2012).

4. Kay, J. *et al.* The Community Earth System Model (CESM) large ensemble project: A community resource for studying climate change in the presence of internal climate variability. *Bull. Am. Meteorol. Soc.* **96**, 1333–1349 (2015).

5. Mullan, A., Stuart, S., Hadfield, M. & Smith, M. Report on the review of NIWA's 'seven-station' temperature series. *NIWA Inf. Ser.* **78**, 175 (2010).

6. Huss, M. & Hock, R. A new model for global glacier change and sea-level rise. *Front. Earth Sci.* **3**, 54 (2015).

7. Stocker, T. F. *et al.* Climate change 2013: The physical science basis (2013).

8. King, A. D., Karoly, D. J. & Henley, B. J. Australian climate extremes at 1.5 C and 2 C of global warming. *Nat. Clim. Chang.* **7**, 412 (2017).

9. Masson-Delmotte, V. *et al.* IPCC, 2018: Summary for Policymakers. In *Global warming of 1.5C. An IPCC Special Report on the impacts of global warming of 1.5C above pre-industrial levels and related global greenhouse gas emission pathways, in the context of strengthening the global response to the threat of climate change, sustainable development, and efforts to eradicate poverty*, 1–32 (World Meteorological Organization, Geneva, Switzerland, 2018).

10. Hock, R. *et al.* High mountain areas. In Pörtner, H.-O. *et al.* (eds.) *IPCC Special Report on the Ocean and Cryosphere in a Changing Climate* (in press, 2019).

11. WGMS. Fluctuations of glaciers database. World Glacier Monitoring Service, Zurich, Switzerland., DOI: 10.5904/wgms-fog-2018-11 (2018).

12. Roe, G. H., Baker, M. B. & Herla, F. Centennial glacier retreat as categorical evidence of regional climate change. *Nat. Geosci.* (2017).

13. Oerlemans, J. Extracting a climate signal from 169 glacier records. *Science* **308**, 675–677 (2005).

14. Oerlemans, J. *The microclimate of valley glaciers* (IGITUR, Universiteitsbibliotheek Utrecht, 2010).

15. Lewis, S. C. & Karoly, D. J. Anthropogenic contributions to Australia's record summer temperatures of 2013. *Geophys. Res. Lett.* **40**, 3705–3709 (2013).

16. Radić, V. & Hock, R. Regionally differentiated contribution of mountain glaciers and ice caps to future sea-level rise. *Nat. Geosci.* **4**, 91 (2011).

17. Marzeion, B., Jarosch, A. & Hofer, M. Past and future sea-level change from the surface mass balance of glaciers. *The Cryosphere* **6**, 1295–1322 (2012).

18. Zemp, M. *et al.* Global glacier mass changes and their contributions to sea-level rise from 1961 to 2016. *Nature* 1 (2019).

19. Xu, J. *et al.* The melting Himalayas: cascading effects of climate change on water, biodiversity, and livelihoods. *Conserv. Biol.* **23**, 520–530 (2009).

20. Huss, M. & Hock, R. Global-scale hydrological response to future glacier mass loss. *Nat. Clim. Chang.* **8**, 135 (2018).

21. Perkins-Kirkpatrick, S. *et al.* The role of natural variability and anthropogenic climate change in the 2017/18 Tasman Sea marine heatwave. *Bull. Am. Meteorol. Soc.* **100**, S105–S110 (2019).

22. Mastrandrea, M. D. *et al.* Guidance note for lead authors of the IPCC fifth assessment report on consistent treatment of uncertainties. (2010).

23. Willsman, A., Chinn, T. & Macara, G. New Zealand glacier monitoring: End of summer snowline survey 2017. Prepared for New Zealand Ministry of Business, Innovation and Employment (2018).

24. Cullen, N. *et al.* An 11-year record of mass balance of Brewster Glacier, New Zealand, determined using a geostatistical approach. *J. Glaciol.* DOI: 10.1017/jog.2016.128 (2017).

25. Purdie, H. *et al.* The impact of extreme summer melt on net accumulation of an avalanche fed glacier, as determined by ground-penetrating radar. *Geografiska Annaler: Ser. A, Phys. Geogr.* **97**, 779–791 (2015).

26. Chinn, T., Fitzharris, B., Willsman, A. & Salinger, M. Annual ice volume changes 1976–2008 for the New Zealand Southern Alps. *Glob. Planet. Chang.* **92**, 105–118 (2012).

27. LaChapelle, E. Assessing glacier mass budgets by reconnaissance aerial photography. *J. Glaciol.* **4**, 290–297 (1962).

28. Mackintosh, A. N. *et al.* Regional cooling caused recent New Zealand glacier advances in a period of global warming. *Nat. Commun.* **8**, 14202 (2017).

29. Oerlemans, J. *Glaciers and climate change* (CRC Press, 2001).

30. Vargo, L. J. *et al.* Using structure from motion photogrammetry to measure past glacier changes from historic aerial photographs. *J. Glaciol.* **63**, 1105–1118 (2017).

31. Cogley, J. G. *et al.* Glossary of glacier mass balance and related terms. *IHP-VII technical documents hydrology* **86**, 965 (2011).

32. Pellicciotti, F. *et al.* An enhanced temperature-index glacier melt model including the shortwave radiation balance: development and testing for Haut Glacier d'Arolla, Switzerland. *J. Glaciol.* **51**, 573–587 (2005).

33. Oerlemans, J. Climate sensitivity of glaciers in southern Norway: application of an energy-balance model to Nigardsbreen, Hellstugubreen and Alfotbreen. *J. Glaciol.* **38**, 223–232 (1992).

34. Berger, A. Long-term variations of daily insolation and Quaternary climatic changes. *J. Atmospheric Sci.* **35**, 2362–2367 (1978).

35. Corripio, J. G. Vectorial algebra algorithms for calculating terrain parameters from DEMs and solar radiation modelling in mountainous terrain. *Int. J. Geogr. Inf. Sci.* **17**, 1–23 (2003).

36. Pellicciotti, F., Raschle, T., Huerlimann, T., Carenzo, M. & Burlando, P. Transmission of solar radiation through clouds on melting glaciers: a comparison of parameterizations and their impact on melt modelling. *J. Glaciol.* **57**, 367–381 (2011).

37. Tait, A. & Liley, B. Interpolation of daily solar radiation for New Zealand using a satellite data-derived cloud cover surface. *Weather. Clim.* **29**, 70–88 (2009).

38. Cuffey, K. M. & Paterson, W. S. B. *The physics of glaciers* (Academic Press, 2010).

39. Brock, B. W., Willis, I. C. & Sharp, M. J. Measurement and parameterization of albedo variations at Haut Glacier d'Arolla, Switzerland. *J. Glaciol.* **46**, 675–688 (2000).

40. Tait, A., Henderson, R., Turner, R. & Zheng, X. Thin plate smoothing spline interpolation of daily rainfall for New Zealand using a climatological rainfall surface. *Int. J. Climatol.* **26**, 2097–2115 (2006).

41. Tait, A. & Macara, G. Evaluation of interpolated daily temperature data for high elevation areas in New Zealand. *Weather. Clim.* **34**, 36–49 (2014).

42. Anderson, B. *et al.* Climate sensitivity of a high-precipitation glacier in New Zealand. *J. Glaciol.* **56**, 114–128 (2010).

43. Rye, C. J., Willis, I. C., Arnold, N. S. & Kohler, J. On the need for automated multiobjective optimization and uncertainty estimation of glacier mass balance models. *J. Geophys. Res. Earth Surf.* **117** (2012).

44. Meinshausen, M. *et al.* The RCP greenhouse gas concentrations and their extensions from 1765 to 2300. *Clim. change* **109**, 213 (2011).

45. Le Quéré, C. *et al.* Global carbon budget 2018. *Earth Syst. Sci. Data (Online)* **10** (2018).

46. Hawkins, E. & Sutton, R. The potential to narrow uncertainty in regional climate predictions. *Bull. Am. Meteorol. Soc.* **90**, 1095–1108 (2009).

47. Hay, L. E., Wilby, R. L. & Leavesley, G. H. A comparison of delta change and downscaled GCM scenarios for three mountainous basins in the United States. *JAWRA J. Am. Water Resour. Assoc.* **36**, 387–397 (2000).

48. Clarke, G. K., Jarosch, A. H., Anslow, F. S., Radić, V. & Menounos, B. Projected deglaciation of western Canada in the twenty-first century. *Nat. Geosci.* **8**, 372 (2015).

49. Zekollari, H., Huss, M. & Farinotti, D. Modelling the future evolution of glaciers in the European Alps under the EURO-CORDEX RCM ensemble. *Cryosphere* **13**, 1125–1146 (2019).

50. Hock, R. Temperature index melt modelling in mountain areas. *J. Hydrol.* **282**, 104–115 (2003).

51. Farinotti, D. On the effect of short-term climate variability on mountain glaciers: insights from a case study. *J. Glaciol.* **59**, 992–1006 (2013).

52. Naughten, K. A. *et al.* Future projections of Antarctic ice shelf melting based on CMIP5 scenarios. *J. Clim.* **31**, 5243–5261 (2018).

53. Randolph Glacier Inventory, A Dataset of Global Glacier Outlines: Version 6.0: Technical Report, Global Land Ice Measurements from Space, Colorado, USA. Digital Media. DOI: https://doi.org/10.7265/N5-RGI-60 (2017).

54. Carenzo, M., Pellicciotti, F., Rimkus, S. & Burlando, P. Assessing the transferability and robustness of an enhanced temperature-index glacier-melt model. *J. Glaciol.* **55**, 258–274 (2009).

Acknowledgements

This work was supported by NIWA Strategic Science Internal Funding of the "Climate Present and Past" project CAOA1901, a subcontract to Victoria University of Wellington from NIWA for "Structure from Motion of Southern Alps glaciers", and a Victoria University of Wellington Doctoral Scholarship. ADK received support from the Australian Research Council (DE180100638). We thank Nicolas Cullen and Pascal Sirguey for sharing Brewster mass-balance data, and Tim Kerr and Heather Purdie for sharing Rolleston mass-balance data. We acknowledge the climate modeling groups that contributed model output to CMIP5, and the groups measuring glacier mass balance that makes up the data in Figure 1. We thank Regine Hock, Shaun Eaves, Claire Lukens, and Ben Marzeion for their input, Trevor Chinn, Andrew Willsman, and Andy Woods for their work on the snowline survey.

Author contributions statement

LJV, BMA, HJH, and RD developed the glacier model. LJV performed the analysis and led the writing. All authors contributed to the design of the study, discussed the results, and contributed to writing of the manuscript.

Competing interests

The authors declare no competing interests.